Spectroscopic investigations of the plasma behavior in a plasma opening switch experiment

M. Sarfaty, Y. Maron, Ya. E. Krasik, A. Weingarten, R. Arad, R. Shpitalnik,
A. Fruchtman, and S. Alexiou
Department of Particle Physics, Weizmann Institute of Science, Rehovot 76100, Israel

The electron density, the electron kinetic energy, the particle motion, and electric fields in a coaxial positive-polarity plasma opening switch (POS) were studied using spectroscopic diagnostics. A gaseous source that injects the plasma radially outward from inside the inner POS electrode was developed. The plasma was locally seeded with various species, desired for the various measurements allowing for axial, radial, and azimuthal resolutions both prior to and during the 180 ns long current pulse. The electron density was determined from particle ionization times and the electron energy from line intensities and time dependent collisional-radiative calculations. Fluctuating electric fields were studied from Stark broadening. The ion velocity distributions were obtained from emission-line Doppler broadenings and shifts. The early ion motion, the relatively low ion velocities and the nearly linear velocity dependence on the ion charge-to-mass ratio, leads to the conclusion that the magnetic field penetrates the plasma early in the pulse. The ion velocity dependence on the axial location were thus used to infer the time dependent axial distribution of the magnetic field, indicating the formation of a relatively high current density at the load-side edge of the plasma. This is expected to cause plasma acceleration towards the load, found to be supported by charge-collector measurements. The fast magnetic field penetration could be explained by mechanisms based on the Hall effect. © *1995 American Institute of Physics.*

I. INTRODUCTION

Investigating the behavior of plasmas carrying high short-duration currents is of major importance for improving the understanding of fundamental plasma physics phenomena, such as magnetic field penetration into plasmas, plasma flow under magnetic and electric fields, and the development of non-neutral regions. Such studies are also essential for improving and scaling up many pulsed-power systems. In particular, plasma opening switches (POS), used to switch high currents into various loads in times of 10^{-8}–10^{-7} s, have been shown to have numerous potential applications in prepulse suppression,[1] pulse shaping,[2,3] and power and voltage multiplication.[4-6] Moreover, the use of POS with microsecond generators allows for generating high power pulses on the nanosecond time scale and avoids certain complications in the conventional high power accelerators.[7-9]

Since plasma opening switches were introduced,[1] much progress in understanding the POS operation has been made due to numerous experimental[10] and theoretical[11,12] studies. The parameters of the plasma preceding the generator pulse were studied using collimated Faraday cups, double-floating probes, visible framing and streak photography, microwave cutoff, and interferometry.[13-15]

During the POS operation, the experimental studies included measurements of the POS upstream and downstream currents and observations of temporal and spatial distributions of x-ray and energetic electron or ion flows.[10,16] Information on the magnetic field evolution in the POS plasma was obtained by the use of magnetic loops inserted into the plasma.[17,18] Investigations of electric fields in a microsecond POS were performed by H_α emission spectral profiles recorded by a Fabry–Perot interferometer.[19] Recently, the time-dependent plasma electron density, averaged over the plasma length was studied for a microsecond POS using interferometry.[20] In spite of the variety of studies performed, it appears that the main phenomena governing the operation of plasma opening switches, such as the time-dependent magnetic field distribution, the plasma flow, and the electron heating are still not well understood. Systematic experimental investigations are still highly required to examine the various underlying theories,[1,11,21-28] and to suggest improvements in the POS operation.

In this study we have focused on developing measurements, which we believe are required for understanding the plasma behavior in plasma opening switches, rather than on improving the performance of the switch. We report on the use of nonintrusive spectroscopic techniques to determine the plasma electron density, electric fields, and the velocity distributions of ions and neutral particles prior to and throughout the 180 ns long current pulse. Absolute line intensities were used to study the absolute densities of plasma constituents and to set a lower bound for the electron energy, which enabled us to determine the electron density from the ionization times of various species seeded in the plasma. It was shown that in determining the electron density using Stark broadening, neglecting the effects of collective fields in the plasma on the emission profiles results in a large error.

High spatial resolution measurements are extremely important for the investigations of high-current carrying plasmas because of the nonequilibrium features of the phenomena, the nonsteady state characteristics of the atomic processes, and the irreproducibility and the spatial nonuniformity in the experiments. To obtain such measurements, we developed a method using laser evaporation to locally seed the plasma with various elements, which allowed for
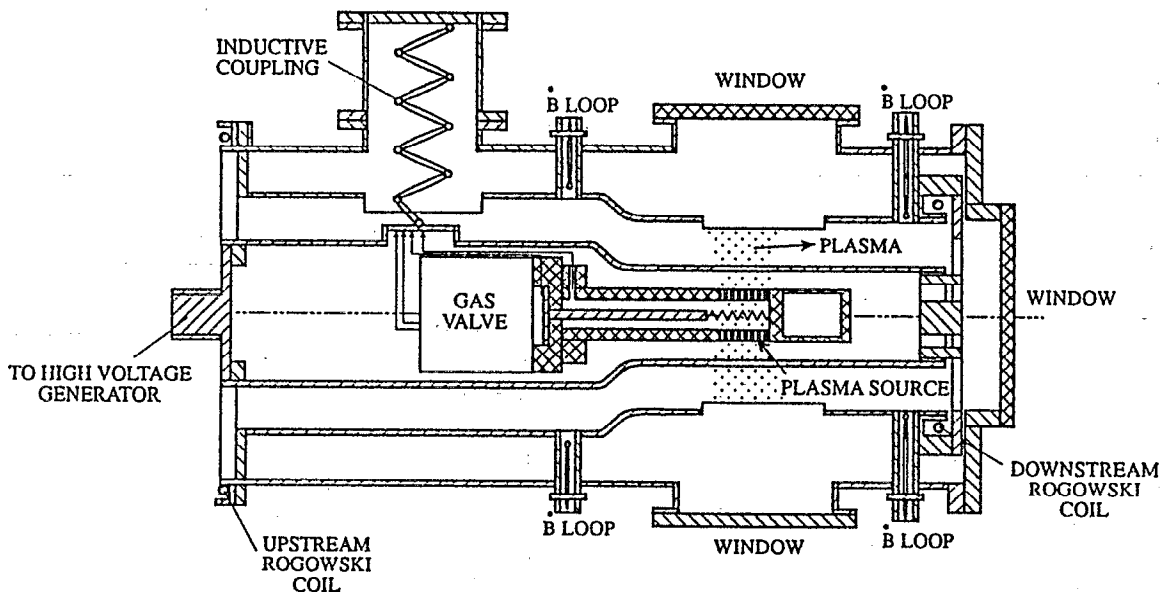
FIG. 1. Schematic illustration of the coaxial plasma opening switch (POS) configuration. The plasma source is mounted inside the inner cylindrical high-voltage electrode, connected to the LC-water-line pulse generator. The power for the gas valve and the plasma source is inductively coupled to the inner electrode. The upstream and downstream currents are measured by Rogowski coils and by two sets of $\dot{B}$ loops, each set has four loops azimuthally separated by 90°, placed upstream and downstream the POS. The voltage at the output of the waterline was measured by a capacitive voltage-divider (not shown in the figure) placed near the water–vacuum interface. The POS chamber has one axial window (in the load side) and four transverse windows for optical accesses.

measurements that are local in r, z, and θ. This also enabled us to select elements whose emission is useful for the various measurements, e.g., of the electron density, the electron energy, and the particle velocities. Also in the present measurements, a high spectral resolution was used in order to discriminate against impurity lines, commonly abundant in pulsed-power experiments, and to observe relatively small Doppler broadenings and shifts.

For systematic investigations, the plasma source should allow for controlling the plasma species and for satisfactory reproducibility. For this reason, we developed a gaseous plasma source[29,30] to be described in detail in a separate publication. The source was so designed to be mounted inside the inner high-voltage electrode of a cylindrical coaxial POS. This allowed for axially symmetric radial plasma injection from inside the inner electrode into the interelectrode gap and for convenient optical accesses into the plasma. The electron density and temperature of the source plasma, as well as the particle velocity distributions prior to the pulse, were determined. In the experiments, we varied the plasma source parameters in order to vary the conduction properties of the switch and the downstream current amplitude.

The spatially resolved ion velocities across the plasma, provided by the measurements based on the plasma-seeding technique developed, showed that the ion motion starts over most of the plasma within the first 40 ns of the pulse, indicating fast magnetic field penetration into the plasma. This conclusion is supported by the relatively low ion velocities and their monotonic dependence on the ion charge-to-mass ratio. Together with the locally determined electron density, the axial ion velocities were used to obtain the forces on the ions, enabling us to suggest a time-dependent magnetic field distribution in the plasma. The axial ion velocities at the

load-side edge of the plasma are found to be significantly higher than in the rest of the plasma, implying a relatively high current density at this edge of the plasma. It is also shown that plasma from the load-side edge of the POS plasma may be accelerated downstream the vacuum line, which is confirmed by charge-collector measurements.

In Sec. II we present the POS system, the diagnostic system, and the plasma source used. Measurements for the two POS parameter regimes studied are given in Sec. III. A discussion of the results is given in Sec. IV, suggesting that the fast magnetic field penetration into the plasma could be explained by mechanisms based on the Hall effect.[21–25] A summary and implications on long time switches are given in Sec. V.

II. THE EXPERIMENTAL ARRANGEMENT AND DIAGNOSTICS

A. The plasma opening switch

In our experiments we use a coaxial configuration shown in Fig. 1. The POS upstream inductance, $L=120$ nH, consists of two coaxial aluminum tubes with a conical transition section varying from outer and inner diameters of 15 and 10 to 10 and 5 cm, respectively. The high-voltage pulse, positive in the present experiments, is delivered by an LC-water-line generator (4.1 kJ, 300 kV, 1 Ω) and applied to the inner electrode giving a peak current of 135 ± 10 kA with a quarter period of 90 ns. The POS load is a shorted coaxial line with outer and inner diameters of 10 and 5 cm, respectively, giving an inductance of 25 nH. Two calibrated Rogowski coils and two sets of four $\dot{B}$ loops azimuthally separated by 90° are used to measure the upstream and downstream currents and the current azimuthal symmetry.

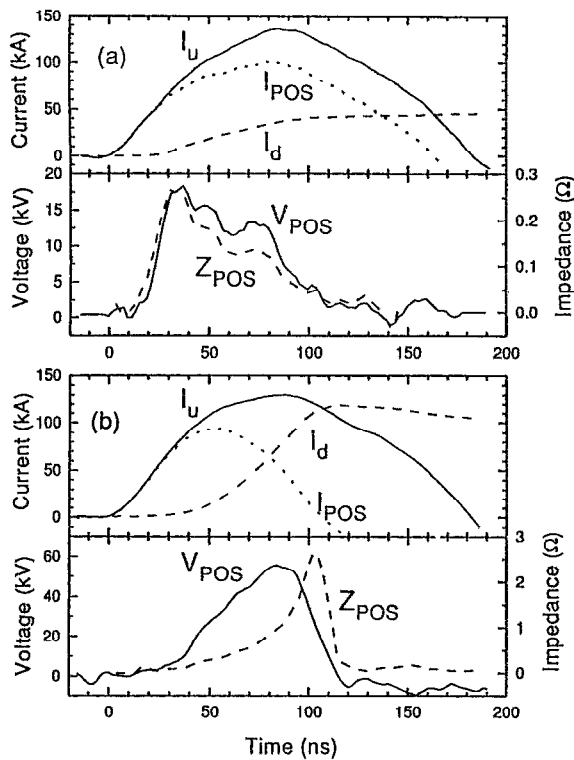Phys. Plasmas, Vol. 2, No. 6, June 1995

Sarfaty et al.   2123

FIG. 2. (a) Waveforms of the upstream current I_u, downstream current I_d, and $I_{pos}=I_u-I_d$ (top). Also given are the anode–cathode voltage in the plasma region, V_{pos}, and the plasma impedance, Z_{pos}, as defined in the text. (b) The same as (a), but for another parameter regime of the POS operation obtained by changing the parameters of the plasma source. For both regimes the inner conductor is charged positive.

The plasma source is installed inside the inner POS electrode and injects the plasma radially outward through a 75% transparent stripped cylindrical anode into the interelectrode region. The downstream current of our POS could be changed in the experiments by varying the period of the flow of the gas in the plasma source to the capillaries (see Sec. II C), and of the time between the gas discharge and the high-current generator pulse. Here, we present data taken with two operation regimes for the POS, whose typical waveforms are given in Figs. 2(a) and 2(b). Shown are the upstream current I_u, the downstream current I_d, and the current $I_{pos}=I_u-I_d$ through the plasma. Also shown are the voltage in the switch region given by $V_{pos}=V_{wl}-L_u(dI_u/dt)\simeq L_d(dI_d/dt)$, where V_{wl} is the water-line output voltage and L_u and L_d are the upstream and downstream vacuum inductances, respectively, together with the POS impedance defined by $Z_{pos}=(V_{pos}/I_{pos})$. In both regimes, the downstream current rises to nearly a plateau at $\simeq 100$ ns indicating a drop in the plasma resistance. In this paper, we mainly discuss measurements for the period until this time. A detailed description of the electrical measurements performed[30] will be described in a subsequent publication.

B. The diagnostic systems

The POS chamber has an optical window that allows for lines of sight parallel to the z axis at various radii and four transverse windows that allow for four radial lines of sight at 90° relative to each other (see Fig. 1). The spectroscopic arrangements used in the experiments are shown in Fig. 3. Two spectroscopic systems that can observe the plasma radially (in the r direction) or axially (in the z direction) are used. Each system includes a 1 m spectrometer equipped with a 2400 grooves/mm grating giving a spectral resolution $\simeq 0.06$ Å. One of these systems images a rectangular region of the plasma onto the spectrograph input slit, and the other system can also image an annular region using a fiber annular-to-linear transformer. The latter arrangement enables us to observe a selected section of the plasma annulus whose minimum length in the azimuthal direction is $\simeq 0.2$ cm ($\simeq 1\%$ of the perimeter). The mirrors M1 and M3 are used to scan in different experiments the POS anode–cathode gap radially and axially. The polarizer and the $\lambda/2$ plate are used for polarization-dependent measurements.

Using a cylindrical lens, the light in the spectrometer exit window is imaged using a cylindrical lens on a rectangular fiber-bundle array, which allows for further dispersion of the light and for varying the dispersion in the experiments. The fiber-bundle array transmits the light to a set of photomultiplier tubes followed by a multichannel digitizer, giving the time dependent line spectral profile in a single discharge with a temporal resolution of 4 ns. The fused-silica optics, the spectrometer, and the photomultiplier tubes allow for sensitivity in the region 2000–7500 Å. Absolute calibration of each spectroscopic system over the entire spectrum (for each fiber channel) was performed using a few intensity-calibrated lamps. The wavelength calibrations of our systems were accurate enough to allow for determining low Doppler line shifts. Also, line profiles observed prior to the current pulse were used to examine the wavelength position of unshifted lines.

Another feature of our diagnostics is the use of a pulsed laser (Nd:YAG, 20 ns, 50 mJ per pulse at $\lambda\simeq 1.06$ μm) to evaporate into the POS interelectrode gap material initially deposited on the anode strips. This allows for seeding the plasma with ions and neutral particles desired for the various measurements. The laser pulse is applied $\simeq 1$ μs prior to the high current pulse producing a seeded conical column between the POS electrodes with a diameter that increases from $\simeq 0.2$ cm near the anode to $\simeq 1$ cm in the middle of the POS gap. The axial location z of the seeded column was varied in the experiments by moving the spot of the laser beam on the anode strip. Observation of light emission from the seeded particles enabled us to obtain measurements that are local in r, z, and θ. The spatial resolution in the z direction is determined by the seeded-column width and that in the r and θ directions, $\simeq 0.05$ and $\simeq 0.5$ cm, respectively, by the imaging optics.

We verified that the plasma seeding did not alter significantly the electron density and temperature in the performed plasma by comparing the line intensities of HI, CI, and CII with and without plasma seedings. Also, using H_β broadening measurements, it was verified that the plasma seeding did not affect the electron density of the prefilled plasma prior to the high current pulse.

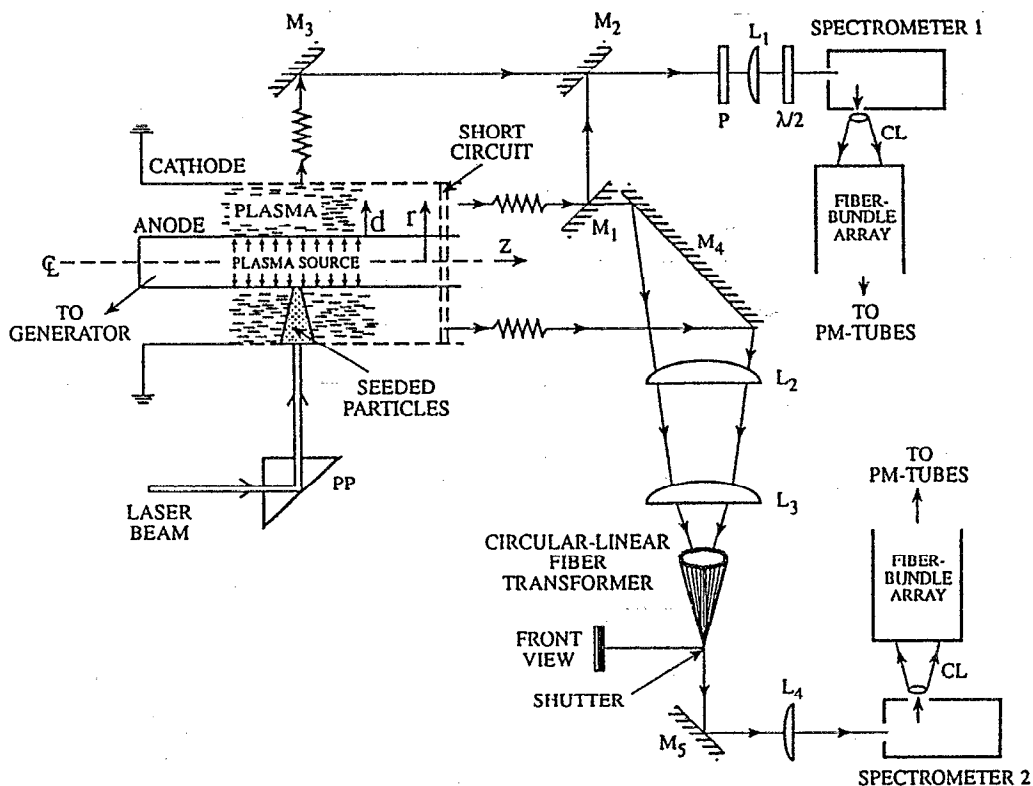In some measurements we observed the radial distribu-

FIG. 3. The diagnostic systems used for the experiments. Light from the plasma is collected axially (through the short-circuit load of the POS) and radially, and is directed onto spectrometer 1 by the use of the mirrors M_1, M_2, and M_3 and the lens L_1. The polarizer P and the $\lambda/2$ plate are used for polarization spectroscopy (see Sec. III D). Spectrometer 2 collects light axially. It can observe a rectangular region or a section of an annular region in the plasma using the lenses L_2 and L_3 and a circular-to-linear fiber transformer. For both spectrometers the light at the exit window is further optically dispersed using the cylindrical lenses CL and is projected onto a rectangular optical-fiber array. The signal transmitted through each fiber is measured by a photomultiplier tube (PM). The laser beam used to evaporate material from the anode surface is directed onto the anode via the prism PP that is used to vary, in different experiments, the axial location of the laser beam spot on the anode. The dotted area shows the column of the seeded particles. Here, r is the radial location and d is the distance from the anode surface.

tions of a line intensity in a single discharge in axial measurements, in which the spectrograph input slit was opened wide enough to allow each fiber bundle to observe a certain radial position in the plasma. Thus the line intensity was observed as a function of time simultaneously for ten radial locations at the expense of the spectral resolution. In the seeding experiments, these measurements gave the radial intensity distributions, local in z, in a single discharge.

C. The plasma source

The plasma gun developed[30] will be described in a subsequent paper. Here, we only present the main information required for the discussions in this paper. The plasma gun operation is based on producing plasma in 144 gas-filled capillaries placed in the walls of a hollow cylindrical tube. The plasma gun is then mounted inside the POS inner electrode and the plasma is injected radially outward. For the measurements reported here, CH_4 was used for the plasma source, producing plasma composed of protons, carbon ions, and neutral hydrogen and carbon.

The electron density and temperature prior to the current pulse were determined from single-probe measurements, microwave cutoff technique, and observations of H_α and H_β spectral profiles.[30,31] The hydrogen line profiles were ana-

lyzed self-consistently to give the electron density and the hydrogen velocity distribution. The electron density thus obtained is shown in Fig. 4(a) as a function of distance from the anode surface.[30,32] The axial plasma length was $\simeq 4$ cm at a radial distance $d \simeq 1$ cm from the anode, as shown by the relative axial density distribution given in Fig. 4(b).[30] The electron density and temperature were uniform within $\pm 15\%$ over the central $\simeq 4$ cm long axial plasma dimension and within $\pm 15\%$ over the azimuthal dimension. The reproducibility of these parameters was found to be $\pm 20\%$. The plasma radial flow velocity was $(1.5 \pm 0.5) \times 10^6$ cm/s.

It was difficult to determine the composition of the plasma in the anode–cathode gap prior to the current pulse. The reason is that the densities of HI, CI, CII, and CIII prior to the pulse, inferred from absolute line intensities and collisional-radiative calculations, are very sensitive to the value of the electron temperature for the considered temperature range. The electron temperature was found to be near 2 eV from carbon–ion line intensities, ionization time of LiI seeded in the plasma, and single probe measurements. Furthermore, the composition is sensitive to the presence of small non-Maxwellian components in the electron energy distribution, also shown to possibly occur in our plasma.[31]

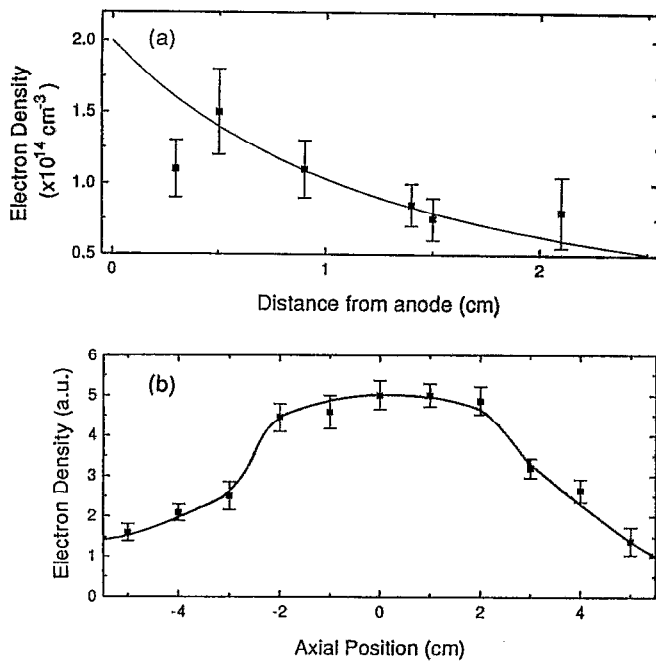Besides CI, CII, and CIII, the performed plasma contains

FIG. 4. (a) The electron density as a function of the distance d from the anode just prior to the current pulse obtained from the H_α and H_β profiles observed axially. The profiles are analyzed self-consistently to give the electron density and the hydrogen velocity distribution. Each data point is an average of a few discharges. The solid line is a calculation of the radial density decrease due to the expansion in both the radial and axial directions. (b) The relative plasma density obtained from double floating probe and Faraday-cup measurements at the time corresponding to the application of the high-current pulse, as a function of the axial location for $d \simeq 1$ cm. The axial center of the plasma source is at $z = 0$ and positive z is towards the load.

FIG. 5. The time-dependent population densities of the LiI $2p$ level and the LiII $2p(^3P^0)$ level, obtained from axial observations of the LiI 6708 Å ($2p-2s$) and the LiII 5485 Å [$2p(^3P^0)-2s(^3S)$] intensities, respectively, for $z = 0$ and $d = 0.7$ cm. Here, lithium was seeded into the plasma and the laser beam was directed to the anode surface at $z = 0$, see Fig. 3.

CIV and CV that could not be spectroscopically observed prior to the pulse because of the low electron temperature. However, CIV and CV provided strong line emission during the pulse either due to electron collisions that are substantially enhanced as a result of the rise in the electron energy, or due to charge-exchange excitations as discussed in Sec. III B.

It was shown that the considerable rise in the HI, CI, and CII line intensities seen during the pulse results from electron excitations. Thus, because of the excitation insensitivity to the relatively high electron energy during the pulse, it was possible to determine the absolute abundances in the plasma of HI, CI, and CII, as given in Sec. III B. From various measurements prior to and during the pulse we concluded that at least one-third of the plasma is protons, with the rest being carbon ions[33] and negligible amount of other impurities.[33]

III. MEASUREMENTS AND DATA ANALYSIS

A. Electron kinetic energy

Bounds on the electron energy were obtained by observing line intensities from various species and transitions. To this end, the plasma was seeded with the desired species in various experiments, which also allowed for local measurements to be obtained, as 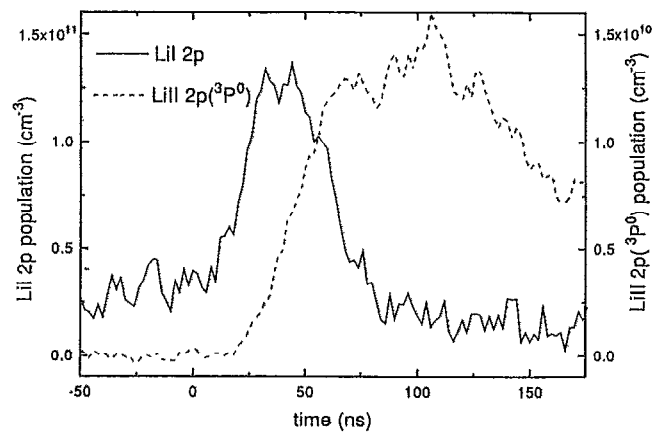described in Sec. II B. In Fig. 5 we present the population of the $2p(^3P^0)$ level of LiII, obtained from the absolute intensity of the 5485 Å line, in an experiment in which the laser illuminated a lithium-coated region of the anode surface. In this figure, $z = 0$ and $d = 0.7$ cm, where z is the axial position relative to the axial plasma center with positive z being towards the load [see Fig. 4(b)], and d is the radial distance from the anode surface (see Fig. 3). It is seen that the line intensity starts rising at $t \simeq 20$ ns and reaches nearly a plateau at $t \simeq 60$ ns.

The ratio between the $2p(^3P^0)$ level density and the total LiII density is obtained using time-dependent collisional-radiative calculations for various electron densities and kinetic energies (since the electron energy distribution may be non-Maxwellian we use the term mean electron energy $\mathcal{E}_e$, rather than electron temperature). Using an upper limit for the total LiII density in the plasma (consistent with the total electron density), these calculations give a lower limit for the density of electrons with energy exceeding that of the $2p(^3P^0)$ level (61 eV). It is found that during the relevant time scale this level is mainly populated through the spin-forbidden transition from the ground state, rather than from the metastable $2s(^3S)$ level. It is also found that a density of at least 5×10^{13} cm^{-3}, i.e., at least 40% of the plasma, see Sec. III B, electrons with energies above 61 eV is required in order to explain the observed $2p(^3P^0)$ density. This result was obtained for $d = 0.2$ to 1.2 cm from the anode.

Note that the LiII density is negligibly affected by the LiI ionization (the LiI density was determined to be too low) or by the slow LiIII recombination. Thus the near constancy of the LiII level population at $t \gtrsim 60$ ns shows that $\mathcal{E}_e$ remains high at this period. The electron energy was further examined by observing the BaIII 3368 Å ($6p[5/2]_3 - 6s[3/2]_2$) line, with an upper level that lies at $\simeq 22$ eV. The time-dependence of the absolute line intensity, together with estimates of the excitation rates,[34] were found to be consistent with the LiII data.

The rise in the electron energy was seen to propagate

Sarfaty *et al.*

from the generator to the load side of the plasma in the period $t \simeq 20$ to $t \simeq 50$ ns. This finding will be discussed in Sec. IV, and was accounted for in the electron-density determination described in the next section.

B. Electron density

The use of Stark broadening in determining the electron density in pulsed-power systems is limited because of the effects of the presence of collective electric fields on the line profiles.[35-39] Evidences for such collective fields were also found in our POS experiment, as described in Sec. III D. Therefore, we determined the electron density during the high-current pulse from the ionization times of various species locally seeded in the plasma. For these measurements, the ionization times must be insensitive to the mean electron energy $\mathscr{E}_e$. Therefore, we selected species such as LiI, BaI, BaII, MgI, and CaI, whose ionization rates saturate when $\mathscr{E}_e$ for most of the electrons in the POS plasma rises to a few electronvolts. The data given in Sec. III A, which show that a substantial fraction of the plasma electrons acquire energies >61 eV, and estimates of classical electron collisionality, show that most of the electrons in the plasma indeed acquire energies above the ionization potentials of these species.

Here, we only present the results for $d \lesssim 1.2$ cm. An example of the LiI $2p$ population during the pulse, obtained from the intensity of the LiI 6708 Å $(2p-2s)$ line observed axially (in the z direction), is shown in Fig. 5. In this figure $z = 0$ and $d = 0.7$ cm. It is seen that the line intensity rises, due to the rise in the mean electron energy, and then decays. The decay in the line intensity could not result from a drop in the mean electron energy, since as discussed in Sec. III A, $\mathscr{E}_e$ remains higher than the $\simeq 2$ eV excitation energy for at least 40 ns after the line intensity starts to decay. We thus conclude that the drop in line intensity is due to ionization. To determine the electron density from LiI, for example, we used an ionization rate of 3×10^{-7} cm^3 s^{-1}, which is obtained from collisional-radiative calculations for electron energies above the ionization potential (5 eV), believed to be accurate to within $\pm 20\%$.[40] Using the ionization times of various species observed, the electron density was shown to be $(1.3 \pm 0.5) \times 10^{14}$ cm^{-3}, over the region $d = 0.2$ to 1.2 cm, and for $z = -1.8$ to 1.4 cm. Since, as mentioned in Sec. III A, the rise of the line intensity was seen to propagate from the generator side to the load side of the plasma, this density is determined for $t = 30-70$ ns at the generator side and for $t = 60-100$ ns at the load side. The uncertainty in n_e mainly results from the irreproducibility in the line intensity time dependence.

Using the ionization times of LiI and BaII, the electron density, was determined as a function of distance from the anode for the region $d \simeq 0.2-1.2$ cm in a single discharge. For these measurements, we employed the wide-slit measurements described in Sec. II B. The radial dependence of the electron density thus obtained and the value of n_e given above were found to be in agreement with those determined prior to the pulse, given in Fig. 4(a). For the region $d > 1.2$ cm, the slow temporal variation of the ionizing species line intensities did not allow n_e to be obtained in this manner.

In principle, the drop in the line intensities could also result from either a drop in the electron density, that causes a drop in the excitation of the radiating level, or from flow of the emitting particles out of the observed region. In these cases, the value given above represents an upper limit for n_e. However, from the constancy of the line intensities of the negligibly ionizing species, such as MgII and BaIII, and from the known particle velocities (see Sec. III C), we inferred that the uncertainty in the determination of n_e due to these factors is within the quoted uncertainty of the electron density.

In our measurements we also observed the absolute densities of excited CIII, CIV, and CV levels. In principle, also these level densities could be used to study the rise in $\mathscr{E}_e$ discussed in Sec. III A, in particular the excitation of the CV level $[2p(^3P^0)]$ that requires an electron energy >300 eV. However, it is possible that the excited-level populations of CIII, CIV, and CV are dominated by processes of charge exchange with hydrogen.[41] Thus as yet we make no inferences from these line emissions on the electron kinetic energy. These possible charge exchange processes also do not allow us as yet to determine the plasma composition.

The observed population densities for the HI, CI, and CII levels $[n = 3, 2p3s(^1P^0)$, and $2s^23p(^2P^0)$, respectively] are shown, however, to be unaffected by charge exchange processes. Therefore, collisional-radiative calculations[42,43] were used to obtain the total densities for these species from the excited-level populations. Using line intensities axially observed and integrated over the entire plasma length, the particle densities at $d \simeq 0.5-1$ cm were found to be $(1.2 \pm 0.7) \times 10^{14}$ cm^{-3}, $(1.2 \pm 0.5) \times 10^{13}$ cm^{-3}, and $(1.2 \pm 0.6) \times 10^{13}$ cm^{-3}, for HI, CI, and CII, respectively. The uncertainties mainly result from the uncertainties in the electron density and the electron energy distribution.

We also consider the possibility of particle ionizations during the pulse. For the electron density in this experiment, the main ionizations are of HI, CI, and CII (the ionization times of higher charge state carbon ions are too long). The largest contribution to ionization comes from HI due to its relatively high density. Using a maximum ionization rate, 4×10^{-8} cm^{-3} s^{-1}, corresponding to an electron temperature $\gtrsim 20$ eV, the HI ionization could cause a rise of a few tens of percents in the electron density during the first 100 ns of the pulse. However, because of the uncertainties in the HI density and in the ionization rate, it is not clear as yet whether ionization causes a significant increase in the electron density in our experiment.

C. Particle velocities

The particle velocity distributions were obtained from the spectral profiles of the Doppler broadened emission lines. The predominance of the Doppler effect on the line profiles was examined by verifying the linear dependence of the profiles on the wavelength using a few lines for the same charge state. Other broadening mechanisms including Zeeman splitting are unimportant relative to the linewidths observed.

Here, we report on two kinds of particle velocity measurements. In the first one, velocities of CI to CV, integrated over the entire axial plasma length, were observed using
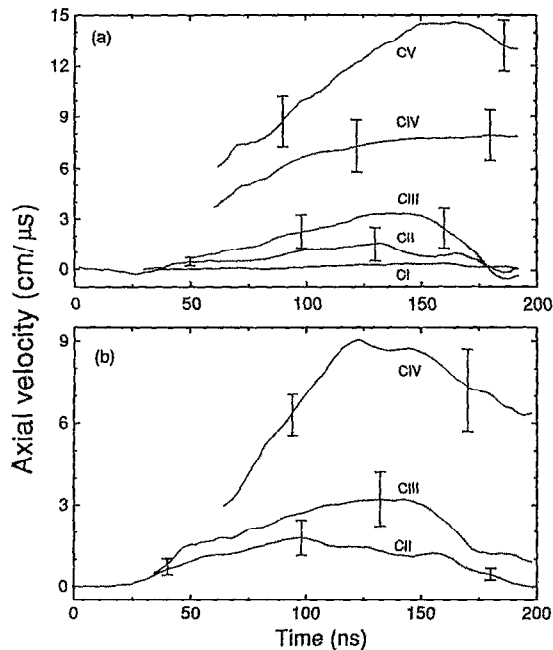
Phys. Plasmas, Vol. 2, No. 6, June 1995

Sarfaty et al.   2127

FIG. 6. (a) The time-dependent mean axial velocities for CI–CV obtained from axially observed Doppler shifts of spectral profiles for $d=0.5$ cm. The lines used for these measurements are 2479 Å $(2p3s(^1P^0)-2p^2(^1S))$, 2512 Å $(2p^3(^2D^0)-2s2p^2(^2P))$, 2297 Å $(2p^2(^1D)-2s2p(^1P^0))$, 2530 Å $(5g-4f)$, and 2271 Å $(2p(^3P^0)-2s(^3S^0))$, for CI, CII, CIII, CIV, and CV, respectively. Positive velocities are towards the load. These data are obtained with the POS parameter regime given in Fig. 2(a). (b) Mean axial velocities for CII–CIV as in (a), obtained with the POS parameter regime given in Fig. 2(b) for $d=0.7$ cm. In both figures, the uncertainty mainly results from the experimental irreproducibility. Each curve is an average over about eight discharges and the error bars give the standard deviation.

axial lines of sight with the resolutions in the radial and azimuthal directions being $\simeq 0.1$ and $\simeq 0.6$ cm, respectively. In the second kind of measurements, in which the plasma seeding was employed, local velocities of singly charged ions were observed.

For most of the axially integrated velocity measurements the line spectral profiles are found to be approximately Gaussian. Using the spectral response of our systems, the true line profiles were deconvolved from the measured ones. The directed velocity in the z direction was obtained from the absolute shift of the line center. Figure 6(a) gives the CI–CV axial directed velocities observed for the POS regime given in Fig. 2(a). The uncertainties in all data here presented mainly resulted from the irreproducibility in the experiments. Thus each measurement was averaged over a few discharges in order to obtain a satisfactory standard deviation. As seen in Fig. 6(a), the CI velocity remains ≲0.5 cm/μs, similar to that observed prior to the pulse,[30] and the ions acquire velocities towards the load that are higher for the higher charge states. These axial observations were performed for $d=0.5-1$ cm from the anode giving similar results.

Note that it is somewhat difficult to obtain from these data the exact scaling of the velocities with the ion charge. The reason is that as discussed above, CI and CII ionize into CII and CIII, respectively, and the excited-level populations for CIII, CIV, and CV may be affected by charge exchange

processes during the pulse, which makes each charge-state group of ions contain ions accelerated with different charges. It appears that the velocity per unit charge, required for the discussion given in Sec. IV, can be obtained most accurately from the velocities of CIV and CV since even under the effects of charge exchange processes, the average charge state of these ions throughout the pulse can be assumed to be 3.5 ± 0.5 and 4.5 ± 0.5, respectively, i.e., the resulting uncertainty is relatively small.

The velocity distributions for CII, CIII, and CIV were also measured for the POS regime given in Fig. 2(b). The mean velocities were found to be similar to those observed for the previous regime, as shown in Fig. 6(b).

These measurements could not give the ion velocity z dependence since they integrate over the axial dimension. In order to obtain the velocity dependence on the axial position, we utilized the plasma seeding technique. More measurements of this kind will be reported in detail elsewhere. Here, we mainly present data for MgII, seeded in the plasma by using the laser to evaporate magnesium deposited on the anode strip.

First, we verified that MgI ionization into MgII could not affect the MgII velocity. To this end, we determined the MgI density from the intensity of the 2852 Å $[3s3p(^1P^0)-3s^2(^1S)]$ line and collisional-radiative calculations,[42] yielding it is $\simeq 1/5$ of the MgII density, i.e., the MgI density is too low to allow the MgI ionization to significantly affect the MgII velocity. Thus, we believe that the MgII velocity observed does reflect the velocity acquired by MgII during the pulse.

MgII velocity measurements were mainly made for the POS regime given in Fig. 2(b). They were made for ten different axial locations of the seeded-MgII column. In Fig. 7(a) we present an example of a velocity distribution obtained from the 2796 Å $(3p-3s)$ line spectral profile for $z=-0.2$ cm. The shifts of such spectral profiles were used to obtain the directed velocities towards the load, shown in Fig. 7(b) for four axial locations at $d=0.7$ cm. It is seen that at the generator-side edge of the plasma [$z=-1.8$ cm, see Fig. 4(b)], the directed velocity remains low, while between $z=-1.4$ to $z+1.0$ cm it rises to $\simeq 2\times10^6$ cm/s at $\simeq 100$ ns. In Fig. 8(a) we present the velocity distribution seen at the load-side edge of the plasma, $z=+1.4$ cm, also for $d=0.7$ cm. Here, the velocity distribution shows relatively high velocities, together with low velocities similar to those seen for z up to 1.0 cm. The velocity distribution given in Fig. 8(a) was satisfactorily fitted by two Gaussian curves that describe the two ion velocity components. The mean velocity for the fast component, averaged over 12 discharges, is plotted in Fig. 8(b), showing peak values that are $\simeq 3$ times higher than that of the slow component. Averaging over a few discharges, the emission intensities of the slow and fast components were found to be about the same. This means that about half the seeded column in the load side of the plasma, i.e., a region $\simeq 0.5$ cm wide in the z direction, can be assumed to move with the higher velocity. Hence, about 13% of the plasma ions in the 4 cm long plasma acquire the high velocities. Note that the ion motion for all axial locations in Figs. 7(b) and 8(b) starts within the first 40 ns of the pulse.
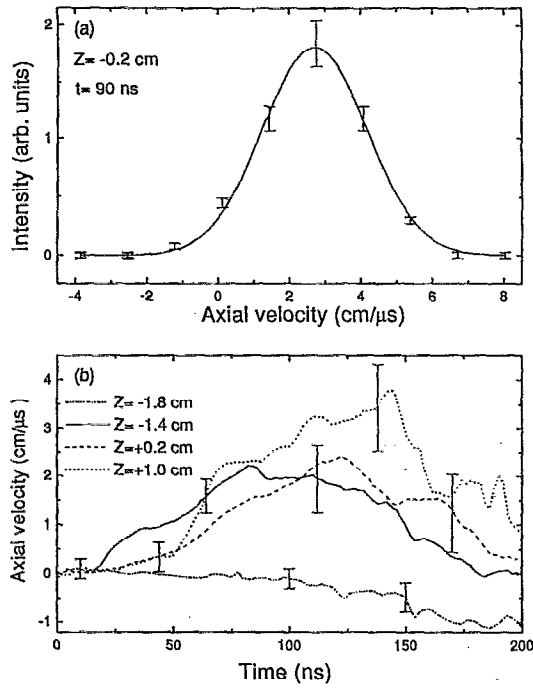
FIG. 7. (a) An example of the MgII velocity distribution obtained from the spectral profile of the MgII 2796 Å $(3p(^2P^0)-3s(^2S))$ line observed axially in the magnesium-seeded experiments for $t=90$ ns, $z=-0.2$ cm, and $d=0.7$ cm. The line is a Gaussian fit to the data. (b) The time-dependent mean axial MgII velocities obtained from the Doppler shifts of the MgII 2796 Å line for $d=0.7$ cm. Given are results for the axial locations: $z=-1.8$ [close to the generator-side edge of the plasma, see Fig. 4(b)], -1.4, $+0.2$, and $+1.0$ cm. Each curve is an average over four discharges and the error bars give the standard deviation.
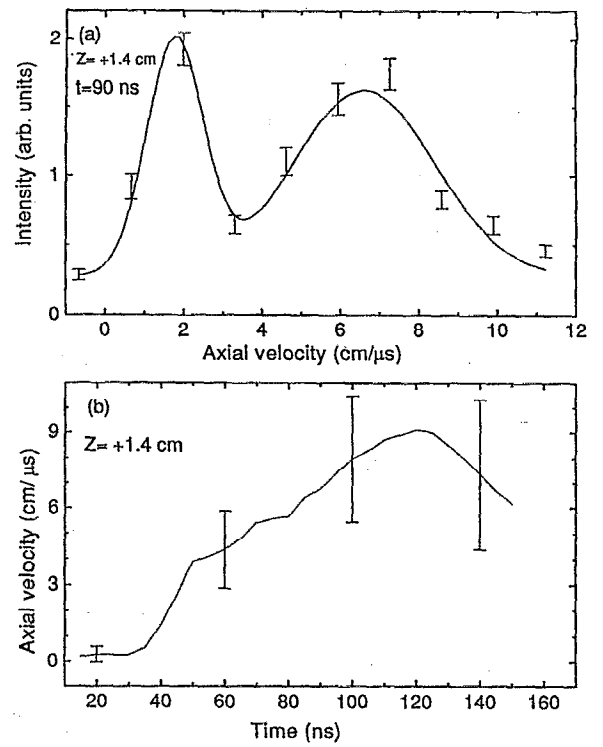

FIG. 8. (a) The MgII velocity distribution obtained from the MgII 2796 Å line spectral profile observed axially for $t=90$ ns, $z=+1.4$ cm, and $d=0.7$ cm. Low-velocity and high-velocity components are seen. The line is a fit of two Gaussian curves to the data. (b) The time-dependent mean axial velocity of the MgII high-velocity component observed at $z=+1.4$ cm and $d=0.7$ cm. The curve is an average over 12 discharges and the error bars give the standard deviation.

The MgII velocities were also measured for $d=0.2$ and 1.7 cm showing phenomena similar to those found for $d=0.7$ cm. We also did measurements of the MgII ion velocity at $z=2.4$ cm, $d=0.7$ cm. Already at this axial position no fast ion component was observed. The light emission of the MgII ions starts to increase and peaks with $\simeq 50$ ns time delay relative to the light emission at $z=1.4$ cm. At this position MgII acceleration towards the generator was observed only at time $\geqslant 120$ ns when the downstream current becomes larger than the upstream current.

Axial velocities for various z locations were also observed for CaII (here, we evaporated CaF_2 from the anode surface) using the CaII 3934 Å $(4p-4s)$ line. The results were found to be similar to those for MgII (except for velocity mass dependence, see below) including the start time of the ion motion and the high velocities in the load side of the plasma. A few local velocity measurements for MgII were also performed for the POS regime given in Fig. 2(a). The results were similar to those described above for the regime in Fig. 2(b), although it appeared that the ion high-velocity component extends over a wider region of the plasma.

We also searched for evidence for relatively high velocities in the axially integrated measurements in which the carbon ion velocities were observed. For this purpose, we observed, for CIII, the wings of the line spectral profile down to less than 10^{-3} of the peak line intensity. Such a detailed spectral profile is shown in Fig. 9 for the CIII 2297 Å

$[2p^2(^1D)-2s2p(^1P^0)]$ line, observed at $d=1.2$ cm for the POS parameter regime given in Fig. 2(a). It is seen that the high-velocity wing of the line is more intense than the low-velocity wing. In order to obtain the relative particle number for each velocity, we assume that the ratio between the upper level and the total CIII densities is similar for all CIII velocities, which probably occurs if this ratio is uniform in z. With this assumption, we subtract the low-velocity wing from the high-velocity wing to obtain the high-velocity component of CIII. This component, shown by the dotted area in Fig. 9, contains $\simeq 10\%$ of the total line intensity, i.e., $\simeq 10\%$ of the CIII in the plasma. This is in a satisfactory agreement with the $\simeq 13\%$ high-velocity component obtained from the MgII measurements. In addition, the high-velocity component for CIII contains ions with velocities $\gtrsim 2\times 10^7$ cm/s, as shown in Fig. 9. Assuming a proportionality of the ion velocity to the charge-to-mass ratio, the fast MgII component should contain velocities $\gtrsim 5\times 10^6$ cm/s, which is also found to agree with the minimum velocities in the fast MgII component shown in Fig. 8(a). Thus the high CIII velocities towards the load appear to be consistent with those found for MgII. We emphasize, however, that in obtaining these results for CIII we assumed that the line intensity is uniform in z. Also, from these measurements the location of the high-velocity ions cannot be known.

The seeding measurements enable us to compare the velocities of different mass and charge-state ions. So far, we

Phys. Plasmas, Vol. 2, No. 6, June 1995
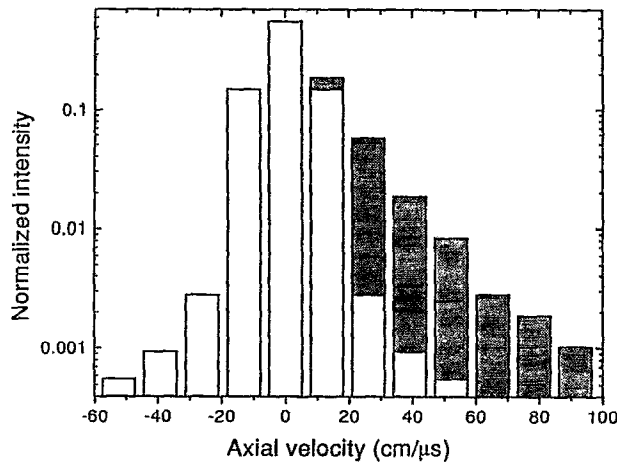
Sarfaty et al.   2129

FIG. 9. The axial velocity distribution of CIII, integrated over the entire plasma length, obtained from the spectral profile of the CIII 2297 Å line, for $t = 100$ ns and $d = 1.2$ cm. The blocks show the light intensity measured by each fiber of the fiber array discussed in Sec. II B. Here, a dispersion of $\simeq 1$ Å per fiber was used in order to observe the spectral profile down to $\simeq 10^{-3}$ of the peak line intensity. The total line intensity is normalized to unity. The dotted regions are the result of a substraction of the low-velocity wing of the distribution from the high-velocity wing. The total area of the dotted regions give the extra light intensity contributed by ions with high velocities towards the load.

FIG. 10. Typical FWHM of the H_α and H_β lines as a function of time, observed axially with the light integrated over the entire plasma length at $d = 1$ cm from the anode.

compared axial velocities of LiII, MgII, CaII, and BaII all measured in the axial center of the plasma. The mean directed velocities at $t = 100$ ns were found to be $\simeq 6 \times 10^6$, 2×10^6, 1×10^6, and 3×10^5 cm/s, respectively, giving an inverse proportionality to the mass within the measurement uncertainty of $\pm 25\%$. We are not studying here the velocity dependence on the charge-to-mass ratio from comparisons of axially integrated to local measurements. The reason is that such a comparison requires a detailed knowledge of the line intensity distributions along the axial plasma dimension, including at the plasma edges, which is not available yet.

The local ion velocity distributions shown in Fig. 7(a) give a velocity spread full width at half maximum (FWHM) $\simeq 2.5 \times 10^6$ cm/s at $t = 100$ ns, which is comparable to the directed velocity. The velocity spreads were seen to rise in time similarly to the directed velocities. We believe the velocity spreads result from velocity spatial variations in the region observed. In the seeding experiments, at $d = 0.7$ cm, the size of this region is $\simeq 1.0$, $\simeq 0.5$, and $\simeq 0.05$ cm in the axial, azimuthal, and radial directions, respectively. Indeed, the velocity spread was observed to be larger relative to the shift, at larger radii where the seeding axial dimension increases. Following the discussion given in Sec. IV, these spatial variations presumably result from variations in the electron and current densities (see discussion in Sec. IV). The velocity spreads for the carbon ions were also found to rise in time similarly to the directed velocities, and to be larger for higher charge states, which is consistent with the claim that the velocity spreads result from spatial variations in the directed velocities. As expected, since the carbon-ion velocity measurements are integrated over the entire axial plasma length, they showed spreads somewhat larger than seen in the local MgII measurements. Consistently, however, also for
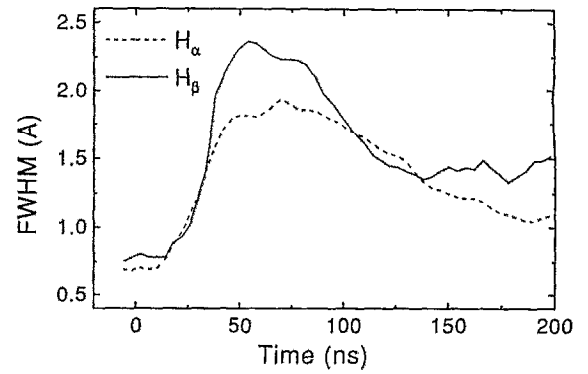
the carbon ions, the velocity spreads were comparable to the respective directed velocities.

Radial ion velocities were observed using radial lines of sight in various axial locations. The velocities obtained were integrated along the radial dimension of the plasma with the resolutions in the z and θ directions being 0.05 and 0.6 cm, respectively. The radial velocities were observed for HI and CI to CV. We note, however, that these measurements suffered from high light intensities from the plasma in the vicinity of the anode. Nevertheless, by comparing axially and radially measured line intensities, we concluded that most of the plasma ions in the radial locations for which the axial velocities were measured ($d = 0.2$ to 1.7 cm from the anode) have radial velocities towards the cathode comparable to their axial velocities towards the load.

D. Electric fields

In order to search for electric fields in the plasma we observed spectral profiles of H_α and H_β. These profiles were observed axially with the measurements being integrated over the entire axial plasma dimension.

The H_β profiles were observed for various radial locations between $d = 0.2$ to 2.3 cm. The line FWHM as a function of time is shown in Fig. 10. The FWHM is seen to rise from 0.80 ± 0.15 Å prior to the pulse to a value of 2.3 ± 0.4 Å at $t = 40$ to 100 ns, followed by a decrease later in the pulse. This finding was seen over the entire plasma region studied. The width during the high current pulse is significantly larger than the width resulting from the thermal Stark broadening due to the plasma-particle fields for the electron density observed during the pulse ($\simeq 1.3 \times 10^{14}$ cm^{-3}, as given in Sec. III A). We suggest that the H_β profile during the pulse is dominated by collective fields in the plasma.

Because of the absence of an unshifted component, the H_β spectral profile is mainly affected by the distribution of the electric microfield amplitude rather than by the field frequency, except for detailed features as the dip and shoulders in the line center. The observed H_β profiles can thus be used to infer the mean amplitude of the collective fields. Because of the H_β width insensitivity to the field frequency, a quasistatic treatment may be used. In this treatment, we assume a Gaussian distribution for the collective electric field to re-

Sarfaty *et al.*

construct the H_β profile. For simplicity, the field distribution is assumed to be isotropic. Also in the calculation, the Doppler broadening due to the 2 eV hydrogen temperature measured prior to the current pulse is accounted for. This procedure yields $\simeq 10$ kV/cm for the mean amplitude of the collective electric field.

The H_α FWHM was also observed to increase significantly during the current pulse, from 0.75 ± 0.1 Å prior to the pulse to 1.8 ± 0.3 Å at $t = 40$ ns to $t = 100$ ns, as shown in Fig. 10. This H_α width is also much larger than the thermal width, accounting for Doppler and ion dynamics,[44] for the electron density observed. Collective fields are thus required to also explain the H_α profile during the pulse. However, for H_α, due to the dominance of the unshifted σ component, high-frequency (nonquasistatic with respect to the inverse HWHM time scale) fields are required to account for the observed broadening. The field frequency[45] should thus be larger than 3×10^{10} Hz. Preliminary analysis indicates that electric fields with an amplitude $\simeq 10$ kV/cm and a frequency $\simeq 10^{11}$ Hz are required to explain both H_α and H_β profiles. More detailed analysis of the H_α and H_β profiles will be reported separately.

In principle, fast hydrogen motion could also affect the hydrogen line broadening. High velocities of hydrogen atoms can result from charge exchange processes. However, analysis of the observed temporal dependence of the H_α and H_β widths, of the absence of shifts for these lines, and of the hydrogen ionization time in the plasma, strongly suggest that the hydrogen motion was too slow to significantly affect the profiles of these lines. Also, the contributions of Zeeman splitting and self-absorption to the line profiles were estimated to be small.

IV. DISCUSSION

A. Ion velocities and magnetic field distribution

The measured ion velocities allow us to study the distribution of the magnetic field in the plasma. If the magnetic field does not penetrate the plasma, the magnetic field pressure is expected to push the plasma at its boundary with a velocity $\simeq V_A$, where $V_A = B/\sqrt{4\pi\rho}$, B is the magnetic field at the vacuum, and ρ is the plasma mass density. The pushing velocity would be within a factor of 2 of this velocity, depending on the pushing mechanism (specular reflection, snow-plow, or a shock wave). The plasma in our experiment is of an electron density $n_e \simeq 1.3 \times 10^{14}$ cm^{-3} and is composed of protons and carbon ions. Its mass density is estimated to be $\rho \simeq 7.5 \times 10^{-10}$ g/cm^3. Thus for $B \simeq 8.7$ kG (using $I_u = 130$ kA and $r = 3$ cm corresponding to $d = 0.5$ cm), the maximum velocity V_A is $\simeq 9 \times 10^7$ cm/s, which reduces to average velocity $V_A \simeq 4.5 \times 10^7$ cm/s taking into account the finite rise time of the magnetic field. As described in Sec. III C, the measured ion velocities are much lower, ranging from 1×10^6 cm/s for CII to 1×10^7 cm/s for CV at $t = 90$ ns. This discrepancy between the ion velocities expected for no magnetic field penetration and the measured ion velocities, implies magnetic field penetration into the plasma, causing a pushing of a larger part of the plasma which results in less momentum gained by each ion.

The assumption of magnetic field penetration is supported by further evidences. One evidence is related to the observed dependence of the ion velocities on their charges. Were the particles specularly reflected by the magnetic piston, their velocities would have been identical for all charges. However, the measured velocities are charge-dependent, higher for higher charge states (see Fig. 6), indicating field penetration. The mass-dependence observed (see Sec. III C), showing lower velocities for the heavier ions, is also consistent with this picture. Magnetic field penetration is expected to result in a linear dependence of ion velocities on the charge-to-mass ratio. However, ionization and charge exchange processes affect this velocity dependence (see Sec. III C). Also, the uncertainties due to the experimental irreproducibility do not allow the exact dependence to be obtained. Nevertheless, the observed monotonic dependence is highly supportive of magnetic field penetration.

The fast field penetration is also supported by the local ion-velocity measurements allowed for by the use of the plasma seeding technique. It is shown in Figs. 7(b) and 8(b) that ions in the entire axial plasma length start to be accelerated as early as $t = 40$ ns. This enables us to conclude that accelerating electric fields, formed by the magnetic pressure, are present across the plasma already at this early time.

In addition to the ion acceleration, ion deceleration is also observed. The mean velocity of the carbon ions is seen in Fig. 6 to decrease in time when the downstream current becomes larger than the upstream current [i.e., for $t > 160$ ns, see Fig. 2(a)]. This ion deceleration averaged over the entire plasma length, resulting from the reversal of the magnetic field pressure caused by I_u becoming lower than I_d, is expected to occur for any field distribution, i.e., even if the magnetic field does not penetrate the plasma. However, the measurements of the local MgII velocities allow us to examine the spatial dependence of the deceleration. Ions on the generator side [see Fig. 7(b) for $z = -1.4$ cm, observed for the parameter regime of Fig. 2(b)] start to decelerate already at $t \cong 90$ ns, long before the total current in the plasma and the magnetic field pressure are reversed. At this time the upstream current starts to decrease [see Fig. 2(b)], suggesting that the early deceleration at the generator side is caused by the formation of reversed currents at this location, resulting in local reversal of the magnetic field pressure. This reversal of the magnetic field pressure at the generator side, prior to the reversal of the magnetic field pressure at the load side, can occur only if the field penetrated the plasma earlier than 90 ns. The early ion deceleration in the generator side of the plasma, provided by the spatially resolved velocity measurements, thus yields additional support to the early field penetration. At $t > 120$ ns, ions decelerate at all axial locations, see Figs. 7(b) and 8(b) for $z = 0.2$, 1.0, and 1.4 cm. As shown in Fig. 2(b), I_{pos} is reversed at $t > 120$ ns. Thus the deceleration at all axial locations at this time results from the reversal of the current and of the magnetic field pressure in the entire plasma length.

We now turn to a quantitative estimate of the magnetic field distribution in the plasma which we obtain from the measured ion velocities by assuming that the ions are accelerated by the Hall electric field. If a current flows through a

Phys. Plasmas, Vol. 2, No. 6, June 1995

Sarfaty *et al.* 2131

region in the plasma, the mean axial velocity of ions of mass M and charge Ze in this region satisfies

$$\frac{dV_z}{dt} = \frac{Z}{M} \frac{1}{8\pi\delta n_e} (B_1^2 - B_2^2). \qquad (1)$$

Here, B_1 and B_2 are the intensities of the magnetic field at the axial boundaries of the region, δ is the width of the region, and n_e is the (assumed uniform) electron density. It is assumed that the ions are uniformly distributed in the region. Equation (1) is obtained from an axial integration of the ion equation of motion over the region, where, as in the rest of this discussion, the plasma pressure is assumed to be much smaller than the magnetic field pressure. It is also assumed that the ion displacement is small relative to δ. Equation (1) is given in a form that is useful in the following analysis.

We first use the measured carbon velocities. Since these velocities are integrated over the entire axial plasma length, we first examine the possibility that the current I_{pos} ($I_{pos}=I_u-I_d$, see Sec. II A) flows uniformly through the plasma. We take B_1 to be B_u, the B field at the generator side, and B_2 to be B_d, the B field at the load side. The intensities of the B field at the generator and at the load sides at a distance r from the axis are calculated using the upstream and downstream currents, I_u and I_d, respectively, that are given in Fig. 2 for the two regimes. We then employ Eq. (1) to calculate the expected mean ion velocities. The calculated velocities of CIV and CV for $t=90$ ns and $d=0.5$ cm for the regime of Fig. 2(a) are 2.5×10^7 cm/s and 3.3×10^7 cm/s, respectively, and for the regime of Fig. 2(b) they are 1.9×10^7 cm/s and 2.6×10^7 cm/s, respectively. These velocities are several times higher than the measured velocities, which are similar for the two regimes, as given in Fig. 6. We chose to compare the calculations to the measurements for CIV and CV since the relative uncertainty in their charge states, even in the presence of charge exchange processes, is sufficiently low (see Sec. III C). The discrepancy between the observed and the calculated velocities for CII and CIII is even larger than for CIV and CV. However, this could result from the ionizations that make CII and CIII accelerate as lower charge states during a fraction of the pulse, as discussed in Sec. III C.

The above analysis, that used the measured carbon velocities, shows that the assumption that the current I_{pos} flows uniformly through the plasma is inconsistent with the data. The local MgII measurements allow us to examine the detailed magnetic field distribution. We, therefore, use Figs. 7(b) and 8(b) and Eq. (1) to calculate the magnetic field distribution at various times for $d=0.7$ cm. At each time $t=40$, 60, 80, and 100 ns, the magnetic field distribution is calculated as follows. The plasma is divided axially into intervals whose centers are at $z=-1.8$, -1.4, -0.2, $+0.2$, $+1.0$ and $+1.4$ cm. The acceleration at each interval is estimated from the axial velocities observed at each z, such as those given in Figs. 7(b) and 8(b). Assuming a density $n_e\cong1.3\times10^{14}$ cm^{-3}, as given in Sec. III A, we calculate the change in B^2 across each interval. Then, starting from the generator side, where the magnetic field B_u is obtained from the upstream current, we calculate B across the plasma. As in writing Eq. (1), we assume in the calculation that the MgII
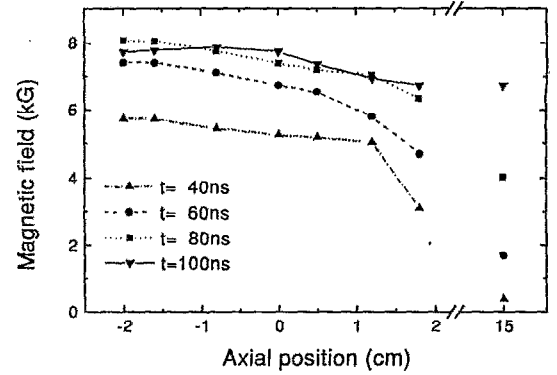

FIG. 11. Axial magnetic field distributions for several times at $r=3.2$ cm (i.e., $d=0.7$ cm from the anode surface) obtained from the axial time-dependent local MgII velocities such as those given in Figs. 7(b) and 8(b). In the calculation, we used an electron density 1.3×10^{14} cm^{-3}, as given in Sec. III A. The data points are connected by straight lines. The points at $z=15$ cm give the magnetic field obtained from the downstream current measured by the Rogowski coil near the shorted load.

displacement is small relative to the length of the interval. This assumption is a good approximation due to the low MgII velocities. Figure 11 describes the approximate magnetic field distribution in the plasma, as it evolves in time. The figure shows fast magnetic field penetration into the plasma and a formation of a relatively high current density at the load-side edge of the plasma. We note that the reversal of the current and the magnetic field pressure at the generator side of the plasma, seen at $t=100$ ns, cause the deceleration of the ions seen in Fig. 7(b) for $z=-1.4$ cm at that time, that we discussed in the above.

As shown in Fig. 11, the calculated magnetic field at the load side of the plasma is larger than B_d, the magnetic field at the load that is obtained from the downstream current. The difference in these values of the magnetic field may result from electron flow in the vacuum section between the plasma and the load[46] or from current through a plasma present in this section. Measurements of a downstream plasma flow are discussed in Sec. IV B. We emphasize that the uncertainties in the ion velocities, the electron density, and the width of the high-current-density layer in the load side of the plasma do not allow us to determine accurately the magnitude of the current that flows outside the main part of the switch plasma.

The data here analyzed were obtained for $d=0.7$ cm. As said in Sec. III C, similar results were obtained for $d=0.2$ and 1.7 cm. Thus we believe the magnetic field distribution here given reflects the distributions in the region between 0.2 and 1.7 cm from the anode. Theoretical studies predict fast magnetic field penetration into the plasma along a narrow region near the anode.[22,28] Such a penetration would not eliminate the acceleration of the unmagnetized parts of the plasma to high velocities. The low ion velocities measured at various distances from the anode make the possibility of penetration only in the neighborhood of the anode very unlikely. The detailed MgII measurements were made for the regime in Fig. 2(b). As said in Sec. III C, few measurements were also performed for the regime of Fig. 2(a) showing similar results, although implying a wider region for the high-velocity ions. Thus it appears that the relatively high current

Sarfaty et al.

density is formed in the plasma load side for the two regimes, i.e., for low and high currents switched to the load. This means that the current density in most of the plasma is also low for the regime of Fig. 2(a), which is consistent with the low axially integrated carbon-ion velocities observed in that regime (see Fig. 6).

Our measurements thus lead to the conclusion that fast magnetic field penetration into the plasma occurs. They also indicate that a high current density is formed in the load side of the plasma early in the pulse.

An important question is the mechanism of the magnetic field penetration. The classical plasma resistivity for an electron temperature of 5 eV is $\simeq 10^{-14}$ s, and the diffusion time τ_d into our 3 cm long plasma is[47]

$$\tau_d = \frac{4\pi L^2}{c^2 \eta} \cong 10^{-5} \text{ s.}$$

This diffusion time is 500 times longer than the field penetration time seen here. Since the electron temperature rises during the pulse, the discrepancy is even larger. Anomalous resistivity due to various instabilities could somewhat shorten this time. However, we suggest that the penetration is associated with to the Hall field mechanism recently studied.[21-25] The condition for the dominance of this penetration mechanism is that the characteristic length is smaller than the ion skin depth. This condition is satisfied for our experimental parameters. The velocity and time for such a penetration are[21-23]

$$V_c \cong \frac{cB}{4\pi e n_e r} = 6 \times 10^7 \text{ cm/s,}$$

$$\tau \cong \frac{4\pi e n_e r}{cB} L = 50 \text{ ns.}$$

In these expressions r is a characteristic length of the nonuniformity. In the numerical evaluation of V_c and τ we used the average magnetic field $B = 5$ kG over the first 50 ns, $n_e = 1.3 \times 10^{14}$ cm^{-3}, $r = 3.2$ cm (corresponding to $d = 0.7$ cm), and the plasma length $L = 3$ cm. Recalling that the characteristic length of the nonuniformity could be smaller than 3.2 cm, this estimate is consistent with the penetration time inferred from the present data.

In order to explain the fast magnetic field penetration by the Hall field mechanism two important questions have to be resolved. First, the Hall-induced penetration is usually associated with a negative polarity POS.[21-23] This is because the Hall effect requires that $n_e r^2$ increases along the electron flow. In our case it is not certain this is true, so this is not fully understood. In relation to this, Gomberoff and Fruchtman have shown that penetration can occur in a positive polarity as well,[24] since even in a positive polarity the electrons may flow along an increasing $n_e r^2$. Moreover, Fruchtman and Rudakov have also shown[25] that the magnetic field pressure can modify the density in such a way, that the field penetration becomes possible.

The second important question is that of the magnetic field energy dissipation. Because of the fast penetration, only a small part of the dissipated energy is expected to be converted to ion kinetic energy. The predicted low ion kinetic energy is consistent with our experimental data. The dissipation per particle expected to result from the magnetic field penetration is approximately $(B^2/8\pi n_e)$. Since the magnetic field seems to penetrate already at $t = 40$ ns, the dissipation available per particle at that time (at $r = 3.2$ cm, $B_u \cong 6$ kG) is expected to be $\cong 5$ keV. At $t = 40$ ns the CIV velocity appears to be $\lesssim 3 \times 10^6$ cm/s (see Fig. 6) and the measured MgII velocity averaged over the entire plasma is $\simeq 5 \times 10^5$ cm/s [see Figs. 7(b) and 8(b)]. Consistent with the data given in Sec. III C, we assume that the ion velocities are proportional to the charge-to-mass ratio and, therefore, the proton velocity is estimated to be $1-1.5 \times 10^7$ cm/s at $t = 40$ ns. This velocity corresponds to a kinetic energy of $\simeq 100$ eV. The heavier ions gain a kinetic energy that is even smaller. Thus the kinetic energy of the ions is only a small part of the dissipated magnetic field energy. Most of the dissipated magnetic field energy is expected to become electron kinetic energy. Note that from the total charge flow the electron ensemble in the plasma can, in principle, be about one time replaced, thus the lower limit for the energy available for each electron can be reduced to $\simeq 2$ keV. The lower bound for the electron kinetic energy here determined is much lower than 1 keV. It has been recently demonstrated[25] that during the magnetic field penetration the magnetic field energy can be dissipated by accelerating electrons in the current channel to a high energy, and these energetic electrons deposit their energy at the anode. The energetic electrons are only located in the narrow current channel, making their relative number small, while most of the electrons, that remain in the plasma behind the current channel, have lower energies. This theory,[25] therefore, may provide an explanation to the question of energy dissipation. The general feature that accelerating the plasma electrons to the anode and replacing them by relatively cold electrons from the cathode provide a way of magnetic field energy dissipation with no electron heating in a collisionless plasma, has also been pointed out by Mendel.[48] Further quantitative investigations of the electron energy distributions, in particular the possible presence of energetic electrons, should be made.

The fluctuating electric fields inferred from the hydrogen line profiles are found to have an amplitude $\simeq 10$ kV/cm and a frequency $> 3 \times 10^{10}$ s^{-1}. Kulsrud et al.[27] and Sudan and Similon[26] discussed the ion acoustic instability driven by drifting electrons. This instability is predicted to fluctuate at ω_{pi} (the ion plasma frequency)[27] and is supposed to saturate[26] at electric fields

$$\frac{T_e}{\lambda_D} \left(\frac{\Omega_e}{\omega_{pe}} \frac{W}{v_t} \right)^{1/3}.$$

Here, T_e is the electron temperature, Ω_e and ω_{pe} are the electron cyclotron and plasma frequencies, λ_D is the Debye length and W and v_t are the electron drift and thermal velocities, respectively. For our parameters the predicted amplitude and frequency of the electric field are a few tens of kV/cm and 10^{10} s^{-1}, respectively. Nevertheless, further measurements and theoretical studies have to be made in order to identify the instabilities responsible for these fields.

Note that the electric field accelerating the ions in the axial direction, obtained from the ion-velocity measurements
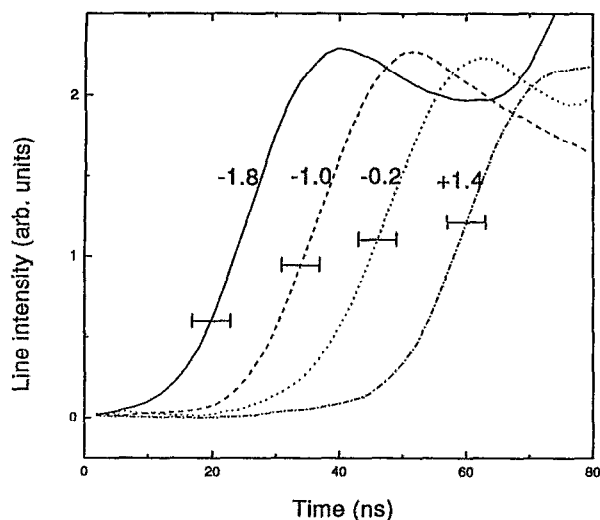
Phys. Plasmas, Vol. 2, No. 6, June 1995

Sarfaty et al. 2133

FIG. 12. The time-dependent intensities of the BaIII 3368 Å ($6p[5/2]_3 - 6s[3/2]_2$) line observed axially in the barium-seeded experiments for $d = 0.8$ cm and for the axial locations $z = -1.8$, -1.0, -0.2, and $+1.4$ cm. The time uncertainty is indicated.
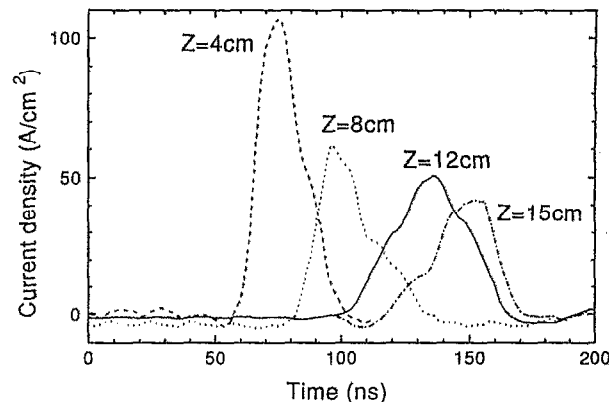

FIG. 13. Ion current density traces measured in a single shot by four collimated Faraday cups (CFC) separated by 90 deg. The CFC are positioned at different axial locations between the plasma and the short-circuit load. A transverse magnetic field prevents electrons from entering the CFC and affecting the measured ion signal.

[Eq. (1)] averaged over $\simeq 10$ ns and 1 cm, is $\simeq 2$ kV/cm. The directed energy that may be delivered to the ions by the higher-amplitude fluctuating fields is expected to be much smaller than the energy delivered by this average field.

The time and z dependence of the line intensities of LiII and BaIII, obtained in the seeding experiments discussed in Sec. III B, showed a rise in the line intensities that propagates axially towards the load, reaching the load-side edge of the plasma within the first 40 ns of the pulse. This is shown in Fig. 12 for BaIII for $d = 0.8$ cm, where the delay in the rise of the line intensity with the distance from the generator-side edge of the plasma, and the intensity rise over the entire plasma within the first 40 ns of the pulse, can be seen. Similar results were observed for d up to 1 cm from the anode. The level excitations for the LiII and BaIII lines require electron kinetic energies of a few tens of electronvolts. This represents a lower limit since higher electron energies are also consistent with the line intensities observed. High energy electrons could be beam of electrons that originate at nonneutral regions in the plasma. The penetration of the magnetic field into the plasma that occurs at the same time raises the possibility that the rise in the electron kinetic energies is associated with currents in the plasma.

B. Downstream plasma flow

The observation of relatively high current density in the load-side edge of the plasma leads to the prediction that plasma in this edge may be accelerated axially towards the load. Due to the nearly linear dependence of the accelerated ion velocity on the charge-to-mass ratio a considerable proton motion is expected. The velocity of the protons in the high current-density region, resulting from the acceleration by the magnetic field pressure there (see Fig. 11) calculated for $t \simeq 60$ ns is $\simeq 10^8$ cm/s. The number of the protons accelerated to this velocity can be estimated from the total number of protons in the 0.5 cm wide region of the high current

density. Since the proton fraction in the plasma is at least 30% (see Sec. II C), the proton density is at least 3×10^{13} cm^{-3}, giving a total number of $\simeq 10^{15}$ protons in this region.

In order to examine this possibility we used magnetically insulated collimated charge collectors to observe axial ion motion in the vacuum section between the switch plasma and the load. In each discharge, four collectors azimuthally separated by 90° were placed at the radial center of the interelectrode gap and at different distances from the switch plasma. Traces observed by the charge collectors are presented in Fig. 13, showing ion signal with a duration $\simeq 40$ ns propagating axially at a velocity $(1.5 \pm 0.7) \times 10^8$ cm/s, obtained from time of flight considerations. The use of positively biased noninsulated collectors showed that electrons were comoving with the ions.

Traces similar to those given in Fig. 13 allowed the total charge collected by the collectors to be calculated, giving $\simeq 1.5 \times 10^{-8}$ C. If this charge is due to singly charged ions, their corresponding number is $\simeq 1.0 \times 10^{11}$. We assume an ion distribution that is nearly uniform in the radial and in the azimuthal directions. We then calculate the total number of ions flowing in the axial direction by multiplying the number of ions collected by the collectors by the area ratio of the interelectrode region and the collectors. The total number of ions thus found is 7×10^{14}.

The agreement between the predicted and observed axial ion velocities towards the load and total number of ions accelerated suggests that these ions are mainly protons that are accelerated from the high-current-density region of the plasma.

At $t \geqslant 40$ ns there is already a magnetic field in the vacuum region between the plasma and the load. The motion of the ions across the magnetic field is not clear as yet. The protons are probably charge neutralized by the comoving electrons and it is possible that this proton plasma carries current. A mechanism of the proton plasma propagation across the magnetic field could be the pushing of the current-carrying proton plasma by the magnetic field pressure. In this case, the current carried by the proton plasma could be part

of the current losses between the POS plasma and the load, discussed in reference to Fig. 11. A second mechanism could be a charge polarization of this proton plasma that allows it to propagate across the magnetic field.[49] Since even at densities $\simeq 10^{12}$ cm^{-3} the condition $n_i m_p c^2 \gg B^2/4\pi$ is satisfied, such a propagation is possible.

C. Observations of electrode plasmas

In our study we also investigated the plasma in the POS gap over a time longer than our current pulse. Plasmas were found to be formed at both electrodes within 50 ns after the beginning of the upstream current, and to flow into the anode–cathode region at a velocity of $1-3\times10^6$ cm/s. The properties of this plasma and its flux were studied in detail[30] using line intensities of various charge states and collision-radiative calculations[42] (as in Ref. 43) and will be published elsewhere. In brief, this plasma was found to be of a relatively high electron density that rises in $\simeq 2$ μs to $\simeq 10^{16}$ cm^{-3} within a few millimeters from the electrodes. It contains singly and doubly charged ions (protons, CII, CIII, AlII, AlIII, FeII, and FeIII) and neutral particles.

Charge-collector measurements of radial ion current through the cathode suggest that the cathode plasma is formed at $\simeq 5$ ns after the beginning of the upstream current, probably due to explosive emission on the cathode surface. In these measurements, magnetically insulated charge collectors were placed behind a 1.5 cm wide slot in the cathode. The charge collectors revealed about 3 ns long ion-current spike, at 5 ± 3 ns after the beginning of the upstream current, besides the commonly observed[10,16] ion current starting a few tens of nanoseconds later. It is possible that the early short-duration ion current results from the formation of strong electric fields in the vicinity of the charge collector screen-box surface, due to the absence of electron emission from that surface, into the current-conducting plasma. The strong electric field would then result in the plasma erosion near this surface. Under this assumption, the total charge collected during the early signal and the plasma density can be used to estimate the width of the eroded plasma region, giving about 100 μm. Assuming a Child–Langmuir charge flow, the current density observed gives a potential drop of $\simeq 1$ kV over that region. The electric field near the plasma near the collector-screenbox surface can thus be estimated to be 100 kV/cm, sufficient to cause explosive emission in this metallic surface. It is plausible that the plasma formation due to the explosive emission[50–52] and the electron emission from this plasma cause the electric field in the vicinity of the collector to drop. This could explain the short duration of the early ion signal. It can be reasonably assumed that the phenomena at the plasma–charge collector boundary are similar to those at the plasma–cathode boundary, which is consistent with the observation of line emission from a plasma near the cathode at $t \lesssim 50$ ns.

To summarize, in our POS, the electrode plasmas, or electrons supplied by these plasmas, may affect the POS properties by causing a reduction in the electric field near the electrodes. In longer-time switches, however, the electrode plasmas can propagate into the POS gap, thus also affecting the plasma composition, density, and ionization processes.

V. SUMMARY

In this study we presented local measurements of the electron density, electron kinetic energy, electric fields, and velocity distributions for up to four times ionized ions in a coaxial plasma opening switch. We have not attempted to study the opening mechanism and to optimize the switch performance. We rather focused on processes that occur during the current conduction by the plasma. The measurements were repeated for two operating regimes of the POS, with low and high currents switched to the load, obtained by varying the parameters of the plasma source used. Similar results were found for all measurements reported here. The early start of the ion motion, the relatively low ion velocities, and the nearly linear dependence of the ion velocity on the charge-to-mass ratio, suggested magnetic field penetration within the first 40 ns of the pulse. Assuming that the ions are accelerated by the Hall electric field, we used the local ion velocity measurements to infer the magnetic field distribution in the plasma. The high ion velocities in the load-side edge of the plasma imply the presence of a relatively high current density at this location in the plasma. If high anomalous resistivity is excluded,[26] it seems that theories based on the Hall field mechanism[21–25] could explain the fast magnetic field penetration observed here. Recent theoretical studies[24,25] allowed for relating the penetration in our experiment to the Hall field mechanism.

The generality of the observed phenomena should be examined by varying the plasma parameters, the POS load, and the POS polarity. More detailed measurements of the ion motion in various radial and axial positions in the plasma and with a higher spatial resolution are highly required. Local Zeeman-splitting measurements of the magnetic field, similar to those described in Ref. 53, are currently underway.[30] For plasmas with significant proton component, the proton dynamics should be studied, perhaps by the study of temporal variations in the local electron density.

The question of energy dissipation is most probably connected to the kinetic energy of the electrons. Our measurements so far only provided a lower bound of a few tens of electronvolts for the electron energy. Further studies are needed in order to estimate the electron kinetic energy.

Our present study raises the possibility of plasma presence and current flow in the transmission line between the plasma and the load. The current flow can be studied in detail by complementing the study of the magnetic field distribution in the plasma with a study of the magnetic field distribution in the region between the plasma and the load.

Our measurements suggest the presence of collective electric fields with an amplitude $\simeq 10$ kV/cm fluctuating with a frequency $>3\times10^{10}$ Hz. The instabilities generating these fields requires further study.[26,27] The ion directed momentum is mainly delivered by the lower-amplitude slowly varying Hall electric fields ($\simeq 2$ kV/cm). Better knowledge of the spatial distributions of these fields and their direction is required for understanding the mechanism of the magnetic field penetration, for investigating non-neutral regions in the plasma, and for determining the plasma resistance.

As said in Sec. III B, ionization processes in our experiment may have not significantly affected the electron density

Phys. Plasmas, Vol. 2, No. 6, June 1995

Sarfaty et al.   2135

during the pulse. However, these processes may play an important role in long-time switches where the ionization rates can be higher (due to the higher electron density) and the times are longer. For such switches, assuming an electron density of 10^{15} cm^{-3} and an electron temperature that rises during the pulse at least to a few tens of electronvolts, we estimate that most of carbon ions ionize into CIV, with a partial ionization of CIV into CV. Thus if the plasma only contains CIII, we expect the electron density to rise to $\lesssim 2$ times its initial value in a period of 1 μs, while if the plasma contains large amounts of neutral particles or singly charged ions, the electron density may rise $\gtrsim 3$ times.

Plasmas were found to form at electrodes early in the pulse, presumably due to explosive emission, causing vanishing of the electric fields at the electrode surfaces. Their observed expansion rate suggest that in long-time switches these plasmas may propagate in the anode–cathode gap, thus affecting the operation of long-time switches, which requires further study.

ACKNOWLEDGMENTS

[1] C. W. Mendel, Jr. and S. A. Goldstein, J. Appl. Phys. **48**, 1004 (1977).

[2] R. A. Meger, R. J. Commisso, G. Cooperstein, and S. A. Goldstein, Appl. Phys. Lett. **42**, 943 (1983).

[3] R. W. Stinnett, D. H. McDaniel, G. E. Rochau, W. B. Moore, E. W. Gray, T. J. Renk, H. N. Woodall, T. W. Hussey, S. S. Payne, R. J. Commisso, J. M. Grossmann, D. D. Hinshelwood, R. A. Meger, J. M. Neri, W. F. Oliphant, P. F. Ottinger, and B. V. Weber, IEEE Trans. Plasma Sci. **PS-15**, 557 (1987).

[4] B. W. Weber, R. J. Commisso, P. J. Goodrich, J. M. Grossmann, D. D. Hinshelwood, J. C. Kellogg, and P. F. Ottinger, IEEE Trans. Plasma Sci. **PS-19**, 757 (1991).

[5] V. M. Bystritskii, A. N. Didenko, S. N. Volkov, I. B. Ivanov, Ya. E. Krasik, and A. V. Petrov, Sov. J. Plasma Phys. **12**, 1178 (1986).

[6] H. Bluhm, K. Bohnel, P. Hoppe, H. U. Karow, and D. Rusch, IEEE Trans. Plasma Sci. **PS-15**, 667 (1987).

[7] B. M. Koval'chyk, G. A. Mesyatz, Sov. Dokl. Acad. Sci. **284**, 857 (1985).

[8] D. D. Hinshelwood, J. R. Boller, R. J. Commisso, G. Cooperstein, R. A. Meger, J. M. Neri, P. F. Ottinger, and B. V. Weber, Appl. Phys. Lett. **49**, 1635 (1986).

[9] G. I. Dolgachev, L. P. Zakatov, and V. A. Skoryupin, Sov. J. Plasma Phys. **13**, 760 (1987).

[10] B. V. Weber, R. J. Commisso, G. Cooperstein, J. M. Grossmann, D. D. Hinshelwood, D. Mosher, J. M. Neri, P. F. Ottinger, and S. J. Stephanakis, Special Issue on Fast Opening Switches, IEEE Trans. Plasma Sci. **PS-15**, 635 (1987), and references therein.

[11] P. Ottinger, S. A. Goldstein, and R. A. Meger, J. Appl. Phys. **56**, 774 (1984).

[12] R. J. Commisso, P. J. Goodrich, J. M. Grossmann, D. D. Hinshelwood, P. F. Ottinger, and B. V. Weber, Phys. Fluids B **4**, 2368 (1992), and references therein.

[13] C. W. Mendel, Jr., D. M. Zagar, G. S. Mills, S. Humphries, Jr., and S. A. Goldstein, Rev. Sci. Instrum. **51**, 1641 (1980).

[14] T. J. Renk, J. Appl. Phys. **65**, 2652 (1989).

[15] L. Veron, R. Boivinet, C. Rouille, B. Etlicher, C. Peugnet, and Dufour, J. Appl. Phys. **71**, 3002 (1992).

[16] P. S. Anan'in, V. M. Bystritskii, V. B. Karpov, Ya. E. Krasik, I. V. Lisitsyn, and A. A. Sinebryukhov, Sov. J. Plasma Phys. **17**, 69 (1991).

[17] B. V. Weber, J. R. Boller, and R. J. Commisso, J. Appl. Phys. **45**, 1043 (1984).

[18] V. M. Bystritskii, Ya. E. Krasik, I. V. Lisitsyn, and A. A. Sinebryukchov, IEEE Trans. Plasma Sci. **PS-19**, 607 (1991).

[19] Yu. P. Golovanov, G. I. Dolgachev, L. P. Zakatov, Yu. G. Kalinin, I. V. Pivinskaya, A. G. Vehakov, and R. V. Chikin, Sov. J. Plasma Phys. **17**, 466 (1991).

[20] D. Hinshelwood, B. Weber, J. M. Grossmann, and R. J. Commisso, Phys. Rev. Lett. **68**, 3567 (1992).

[21] K. V. Chukbar and V. V. Yan'kov, Sov. Phys. Tech. Phys. **33**, 1293 (1988); Ya. L. Kalda and A. S. Kingsep, Sov. J. Plasma Phys. **15**, 508 (1989).

[22] A. V. Gordeev, A. V. Grechikha, A. V. Gulin, and D. M. Drozdova, Sov. J. Plasma Phys. **17**, 381 (1991).

[23] A. Fruchtman, Phys. Fluids B **3**, 1980 (1991); A. Fruchtman and K. Gomberoff, *ibid.* **4**, 117 (1992).

[24] K. Gomberoff and A. Fruchtman, Phys. Fluids B **5**, 2841 (1993).

[25] A. Fruchtman and L. I. Rudakov, Phys. Rev. Lett. **69**, 2070 (1992); Phys. Rev. E **50**, 2997 (1994).

[26] R. N. Sudan and P. L. Similon, in *Proceedings of the 7th International Conference on High Power Particle Beams*, Karlsruhe, Germany, 1988 (Nuclear Research Center, Karlsruhe, Germany, 1988), Vol. 1, p. 416; L. I. Rudakov, C. E. Seyler, and R. N. Sudan, Comments Plasma Phys. Controlled Fusion **14**, 171 (1991).

[27] R. M. Kulsrud, P. F. Ottinger, and J. M. Grossmann, Phys. Fluids **31**, 1741 (1988). See National Technical Information Service Document No. PB92-206168 (J. M. Grossmann, C. R. DeVore, and P. F. Ottinger, in Proceedings of the 9th International Conference on High Power Particle Beams, Washington, D.C. 1992, Vol. 1, p. 559). Copies may be ordered from the National Technical Information Service, Springfield, VA 22161.

[28] H. A. Davis, R. J. Mason, R. R. Bartch, J. B. Greenly, and D. J. Rej, in Ref. 27, p. 615.

[29] R. Arad, R. E. H. Clark, G. Dadusc, G. Davara, R. E. Duvall, A. Fisher, V. Fisher, M. E. Foord, A. Fruchtman, L. Gregorian, Ya. E. Krasik, C. Litwin, Y. Maron, L. Perelmutter, M. Sarfaty, E. Sarid, S. Shkolnikov, R. Shpitalnik, L. Troyansky, and A. Weingarten, Rev. Sci. Instrum. **63**, 5127 (1992).

[30] M. Sarfaty, Ph.D. thesis, Feinberg Graduate School, Weizmann Institute of Science, Israel, 1993; M. Sarfaty, R. Arad, Ya. E. Krasik, Y. Maron, B. Pereiaslovets, S. Shkolnikov, R. Shpitalnik and A. Weingarten, in *Abstracts IEEE (The Institute of Electrical and Electronics Engineers, Inc.) International Conference on Plasma Science*, Vancouver, Canada, 1993 (Institute of Electrical and Electronic Engineers, New York, 1993), p. 113.

[31] R. Arad, M. Sc. thesis, Feinberg Graduate School, Weizmann Institute of Science, Israel, 1993; M. Sarfaty, Ya. E. Krasik, R. Arad, Y. Maron, A. Weingarten, and A. Fisher, in *Abstracts IEEE International Conference on Plasma Science*, Tampa, Florida, 1992 (The Institute of Electrical and Electronics Engineers, New York, 1992), p. 166.

[32] M. Sarfaty, Ya. E. Krasik, R. Arad, A. Weingarten, S. Shkolnikov, and Y. Maron, in Ref. 27, p. 633; A. Weingarten, M.Sc. thesis, Feinberg Graduate School, Weizmann Institute of Science, Israel, 1993.

[33] M. Sarfaty, R. Arad, Ya. E. Krasik, Y. Maron, B. Peryaslovetz, S. Shkolnikov, R. Shpitalnik, and A. Weingarten, Bull. Am. Phys. Soc. **38**, 1895 (1993).

[34] Yu. Ralchenko (private communication, 1993).

[35] H. J. Kunze and H. R. Griem, Phys. Rev. Lett. **21**, 1048 (1968).

[36] G. V. Sholin and E. A. Oks, Sov. Phys. Dokl. **18**, 254 (1973).

[37] H. G. Griem, *Spectral Line Broadening by Plasmas* (Academic, New York 1974).

[38] G. Bekefi, C. Deutch, and B. Yakobi, in *Principles of Laser Plasmas*, edited by G. Bekefi (Wiley, New York 1976).

[39] E. Sarid, Y. Maron, and L. Troyansky, Phys. Rev. E **48**, 1364 (1993).

[40] H. Tawara, T. Kato, and M. Ohnishi, At. Data Nucl. Tables **36**, 167 (1987);

D. Leep and A. Gallagher, Phys. Rev. A **10**, 1082 (1974), and references therein.

[41] D. Dijkamp, D. Ciric, E. Vlieg, A. de Boer, and F. J. de Heer, J. Phys. B **18**, 4763 (1985); S. Bienstock, T. G. Heil, C. Bottcher, A. Dalgarno, Phys. Rev. A **25**, 2850 (1982); R. A. Phaneuf, *ibid.* **24**, 1138 (1981).

[42] M. E. Foord, Y. Maron, and E. Sarid, J. Appl. Phys. **68**, 5016 (1990).

[43] Y. Maron, L. Perelmutter, E. Sarid, M. E. Foord, and M. Sarfaty, Phys. Rev. A **41**, 1074 (1990).

[44] J. Seidel, in *Spectral Line Shapes*, Vol. 6, edited by L. Frommhold and J. Keto, AIP Conf. Proc. No. 216 (American Institute of Physics, New York, 1990).

[45] D. H. Oza, R. L. Greene, and D. E. Kelleher, Phys. Rev. A **37**, 537 (1988).

[46] L. E. Aranchuk, V. M. Babykin, A. S. Chernenko, and A. S. Chuvatin, Sov. J. Plasma Phys. **17**, 317 (1991); C. W. Mendel, Jr., M. E. Savage, D. M.

Zagar, W. W. Simpson, T. W. Grasser, and J. P. Quintenz, J. Appl. Phys. **71**, 3731 (1992).

[47] N. A. Krall and A. W. Trivelpiece, in *Principles of Plasma Physics* (McGraw-Hill, New York, 1973).

[48] C. W. Mendel, Jr. (private communication, 1993).

[49] W. Peter and N. Rostoker, Phys. Fluids **25**, 730 (1982).

[50] S. P. Bugaev, E. A. Litvinov, G. A. Mesyats, and D. I. Proskurovskii, Sov. Phys. Usp. **18**, 51 (1975).

[51] P. A. Miller, J. W. Powkey, and T. P. Wright, Phys. Rev. Lett. **35**, 940 (1974).

[52] M. Yu. Krendel, E. A. Litvinov, G. E. Ozur, and D. I. Proskurovskii, Sov. J. Plasma Phys. **17**, 825 (1991).

[53] Y. Maron, E. Sarid, E. Nahshoni, and O. Zahavi, Phys. Rev. A **39**, 5856 (1989).